IEEE Access
Multidisciplinary | Rapid Review | Open Access Journal

Received February 24, 2020, accepted March 28, 2020, date of publication April 3, 2020, date of current version April 20, 2020.

Digital Object Identifier 10.1109/ACCESS.2020.2985386

A Dual VSG-Based M3C Control Scheme for Frequency Regulation Support of a Remote AC Grid Via Low-Frequency AC Transmission System

MUSTAFA AL-TAMEEMI[1], JIA LIU[1], (Member, IEEE), HASSAN BEVRANI[2], (Senior Member, IEEE), AND TOSHIFUMI ISE[3], (Member, IEEE)

[1]Division of Electrical, Electronic and Information Engineering, Graduate School of Engineering, Osaka University, Osaka 565-0871, Japan
[2]Department of Electrical Engineering, Smart/Micro Grids Research Center, University of Kurdistan, Sanandaj 66177-15175, Iran
[3]Nara-Gakuen Incorporated Educational Institution, Nara 636-8503, Japan

Corresponding author: Jia Liu (liu@pe.eei.eng.osaka-u.ac.jp)

This work was supported by the JSPS KAKENHI under Grant JP19H02131.

ABSTRACT This paper proposes a low-frequency ac (LFAC) transmission system capable of providing frequency regulation support for a remote ac grid aiming at enhancing its frequency stability. The LFAC transmission system using modular multilevel matrix converters (M3Cs) for a direct ac-ac conversion is receiving noticeable attention as an alternative solution for a long-distance transmission system. One of its potential applications is the system connection between a large ac grid and a remote ac grid, whereas the latter usually suffers from a fluctuant frequency due to lack of inertia. The core of this work is addressing a novel control scheme of the remote ac grid-side M3C, which makes both interactions with the LFAC system and the remote ac grid behave like a synchronous generator using a dual virtual synchronous generator (VSG) control scheme. This control scheme can enhance the frequency regulation in the remote ac grid, which the existing control schemes cannot provide. Average dc capacitor voltage versus active power (V_{ave}-P) droop control is proposed to coordinate the power flow between the VSG controls applied in both sides of the M3C. To demonstrate the problem of the existing control scheme, as well as the benefits offered by the proposed control scheme, transient performance including load variation and fault events in the remote ac grid is studied and examined in the EMTDC/PSCAD software environment.

INDEX TERMS Frequency control, low-frequency ac transmission, modular multilevel matrix converter, power control, power grids, power transmission, remote grid, virtual synchronous generator.

I. INTRODUCTION

The connection to a remote ac grid via high voltage ac (HVAC) system using utility frequency requires a long transmission line, which is expensive, poor efficiency and of low transient stability. If the remote ac grid operates as an isolated grid, it will be suffered from a large frequency fluctuation during transition due to relatively small power rating of generators and low inertia compared to the occurred loading variation. This problem becomes more severe if generators in the remote ac grid are replaced by power-electronics-interfaced generators [1], [2].

Voltage source converters based high voltage direct current (VSC-HVDC) systems are proposed to connect the remote ac grid with the main grid in order to overcome the conventional HVAC system limitations. In order to enhance the VSC-HVDC systems to provide frequency regulation support for the remote ac grid, they were controlled in a manner to provide an inertial response by incorporating inertia emulation control strategies such as using the kinetic energy stored in the DC-link capacitor [3]. It is also reported that a proper frequency regulation scheme can be added to the conventional phase-locked loop (PLL) synchronized VSC-HVDC,

The associate editor coordinating the review of this manuscript and approving it for publication was Tariq Masood.

thus help the latter to self-maintain the frequency stability in the remote ac grid [4].

An attractive control scheme emphasizes on enabling the converter to behave like a synchronous generator (SG) by integrating an equivalent swing equation into the controller [5], [6]. Meanwhile, the concept of the virtual synchronous generator (VSG) [7], or virtual synchronous machine (VSM) [8], is proposed for distributed generators (DGs) for a similar purpose. This concept is further developed in [9]–[16]. It is thus straightforward to apply the VSG control to VSC-HVDC for providing frequency regulation for a two-area ac grid [17]. Consequently, VSC-HVDC system installation continued to increase to include offshore wind power connection to weak ac grid [18], asynchronous power grid interconnection [19], and long-distance transmission for onshore windfarms (WFs) [20].

Despite all merits offered by an HVDC system, still, its protection reliability, as well as its control complexity level are questionable. For example, due to the absence of the zero-crossing points, it is difficult to quickly disconnect a faulty line. Moreover, the HVDC circuit breakers are based on power electronic technology, in which they are vulnerable to thermal failure. Therefore, the protection of an HVDC system is still an immature technology that requires further development and research [21].

To respond to the limitations of both HVAC and HVDC systems, a low-frequency ac (LFAC) transmission system [22], [23], [24], also referred to as fractional frequency transmission system (FFTS) [25], is being proposed nowadays as an additional transmission solution [26]. This system transmits the power at a lower frequency ranging about 1 Hz – 60/3 Hz and offers significant advantages. Compared with the HVDC system, the LFAC system has zero-crossing points, thus, the protection is more advantageous. The LFAC system reactance is lower than that of the conventional HVAC transmission, which can be beneficial in two ways. First, the LFAC system allows more maximum transmission power, and second, it improves transient stability compared to the conventional HVAC system, owing to comparatively larger power angle curve [27], [28].

Due to the mentioned technical advantages, the LFAC system is ongoing to be studied in many works. These works employ the LFAC system using various ac/ac converters, circuit configurations, and topologies. For example, in [29], the cycloconverter introduced for LFAC system focusing on offshore wind power application, and a multiterminal configuration using cycloconverter is presented in [30]. However, the use of the cycloconverter presents some fatal drawbacks, such as heavy harmonics, and low power factors. A back-to-back voltage source converter (BTB-VSC) is also introduced for the LFAC system [31]. This device alleviates some technical concerns when connecting to a mainland grid owing to the enhanced dynamic control over both active and reactive power, and a more sophisticated switching pattern reduces the need for lower order harmonic filters. However, the BTB-VSC such as BTB modular multilevel converter (MMC) are based on three stages (ac/dc/ac) of conversion for one station, which requires numerous converter cells and a bulky DC-link capacitor. Therefore, using such a converter will reflect on high cost and complex control compared to a direct ac/ac conversion. In [25], the LFAC system is introduced using a Modular Multilevel Matrix Converter (M3C). The M3C has been successfully proposed in the wind energy conversion system (WECS) as a frequency converter [32]. The M3C is considered as the next generation ac/ac converter due to its technical advantages, which are, easy scalability, smaller capacitance required, high power quality, and controllable power factor on both sides.

Previous works on the LFAC systems focus either on controlling the power flow or employing the VSG concept on the LFAC side [26], [30]. The latter enables the LFAC side of the M3C to behave like an SG and to provide synchronized power, and thus, has succeeded in forming a multiterminal LFAC (MT-LFAC) system. However, the existing control scheme for the utility side of the M3C is based on controlling the power on a dq coordinate frame [26]. When the LFAC system is used to connect a remote ac grid to the main grid, such a control scheme cannot provide an inertial response to the remote ac grid.

To highlight the contribution of this work, to the authors' best knowledge, the M3C-LFAC system has not yet been introduced to address the frequency control issue of a remote ac grid. Therefore, this paper proposes a frequency regulation support for the LFAC system interconnecting a remote ac grid to the main grid using M3Cs as ac/ac converters. This is realized by using a dual VSG control for the M3C at the remote ac grid side. Each VSG has a different task. The LFAC side VSG provides a synchronized power for the LFAC network to enable a potential multi-terminal operation [26]. Moreover, it maintains the cell dc capacitor voltage constant. Meanwhile, the remote ac grid side VSG is employed to enable the converter to mimic the dynamics of the SG and thus to provide a robust frequency regulation support for the remote ac grid. The concept of this work is stimulated by the works on VSC-HVDC system with inertia emulation [5]; however, the feature of our proposed M3C-LFAC system removes the limitations of using an HVDC transmission system. In other words, this work can be used as an alternative solution for better providing the existed services by the HVDC system.

It is noteworthy to mention that, applying a dual VSG for controlling both M3C sides is not straightforward. Due to the intentional slow response of VSG control in both sides, it is difficult to apply conventional average dc capacitor voltage control, which requires a fast inner current control loop. Therefore, in this work, we propose an average dc capacitor voltage versus active power (V_{ave}-P) droop control method integrated into the LFAC side VSG control, to achieve the balance between input and output M3C active powers and thus to maintain the capacitor voltage while reacting fast enough to support the dynamics of a remote ac grid. Such control technique, to the authors' best knowledge, has never been applied, particularly with the VSG for M3C control.

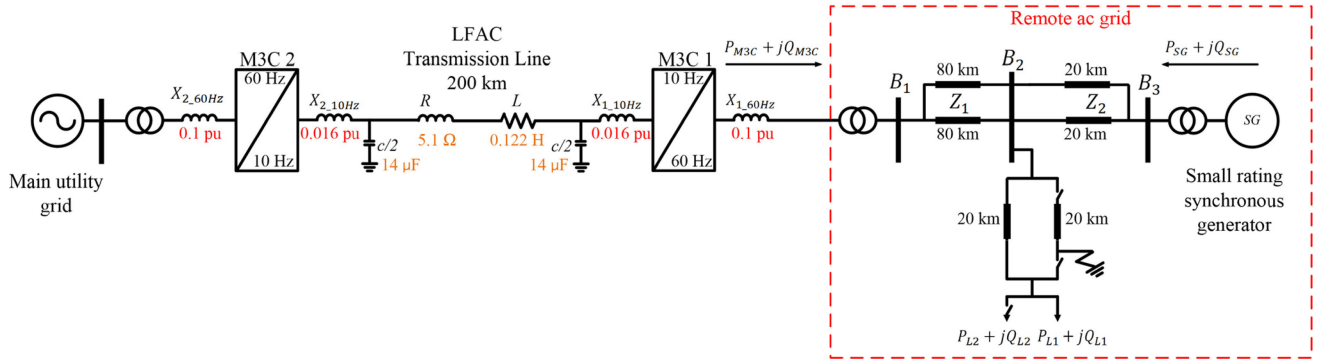

FIGURE 1. Single-line diagram of a point-to-point M3C-LFAC system.

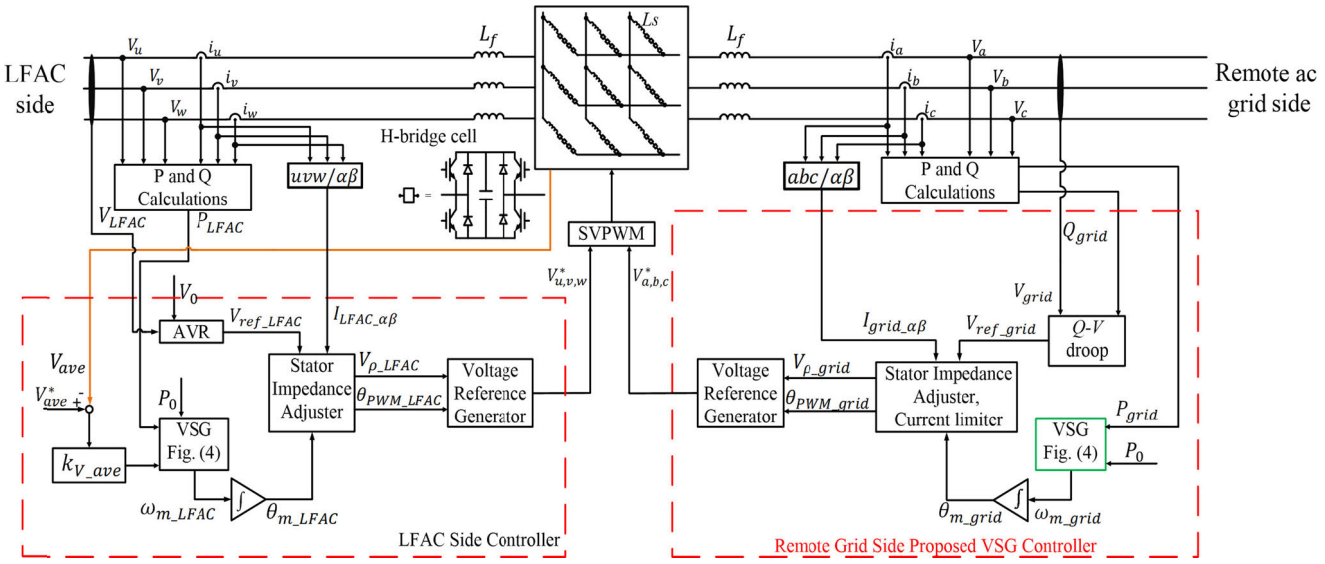

FIGURE 2. Main circuit and the proposed control system of M3C 1.

The rest of the paper is organized as follows: Section II describes the entire circuit configuration of the proposed system. Section III discusses the conventional and the proposed M3C control schemes for both the remote grid and the LFAC sides. Section IV validates the proposed system with numerical simulations. Conclusions are discussed in Section V.

II. M3C-LFAC SYSTEM CONFIGURATION

A case study of point-to-point M3C-LFAC configuration is presented in this paper to demonstrate our proposed control scheme, which is illustrated in Fig. 1. It is a combination of two stations, each station is driven by an M3C that acts as a frequency converter to convert the low-frequency ac (10 Hz) to 60 Hz in order to interface with the grid. It is explained in [25] and [33], that the selection of the operating low frequency can affect the transmission distance, the transformer design on the LFAC side, the number of the submodule capacitor of the M3C, and the capacitive charging current. Therefore, in this work, the 10 Hz frequency is selected merely to operate the LFAC system. The discussion on the optimal frequency of LFAC system is beyond the scope of this paper.

It is noteworthy to mention that this configuration can be easily extended to a multi-terminal LFAC system as proposed in [26]. The focal point of this research is the remote ac grid (60 Hz) side of M3C 1 as an interface to the LFAC system to show the advantages of the proposed control compared to the existing control schemes for M3C-LFAC system. Therefore, the control scheme of the main utility side M3C (M3C 2), which uses the existing control scheme [26], is omitted in this paper.

III. THE CONTROL SYSTEM OF M3C

A. CONFIGURATION OF THE M3C

Fig. 2 shows the circuit configuration and the entire control scheme of M3C 1. The M3C circuit consists of nine arms, each arm has four H-bridge cells connected in series and these cells connect the grid side to the LFAC side. In practical application, each arm consists of hundreds of H-bridge cells considering the voltage level, thus the filter inductance L_f can be quite small. In this study, the number of cells is reduced to four for simplicity and less computational time of the simulation. Moreover, small inductors called arm inductors (L_s) are connected with each converter arm in order to suppress the

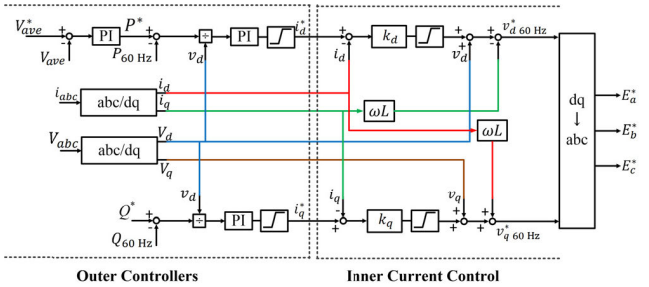

FIGURE 3. A block diagram of the M3C remote ac grid side conventional control.

current flowing at the timing of commutation between those arms. The overall control of the M3C is shown in Fig. 2. The control scheme can be divided into two parts; the grid side (60 Hz side) control part, and the LFAC side (10 Hz side) control part. From Fig. 2, the grid side is controlled by using either a VSG control or a conventional control based on PI controllers on the *dq* coordination frame as shown in details in Fig. 3.

B. CONVENTIONAL CONTROL OF THE M3C

Fig. 3 shows the conventional remote ac grid side controller of the M3C that combines both the outer controller (on the left) and the inner controller (on the right). A synchronous *dq* reference approach is conventionally employed to guide the M3C control [34], [35]. A positive sequence of three phase voltages V_{abc} and currents i_{abc} is transformed to the *dq* components using the Park's transformation, with the phase angle (θ_{PLL}) obtained from the PLL.

The outer controllers include controlling active and reactive power of the grid side. The active and reactive power that the M3C injects into the grid are expressed in dq-axis as

$$P_{60Hz} = \sqrt{2/3} * (v_d i_d + v_q i_q) \tag{1}$$

$$Q_{60Hz} = \sqrt{2/3} * (v_q i_d - v_d i_q) \tag{2}$$

Both active and reactive powers can be controlled using PI controllers on the *dq* coordinate in the outer controllers. However, to keep the active power balance between both sides, instead of directly controlling the active power, in [26], the average dc capacitor voltage V_{ave} is controlled, which is calculated from all the H-bridge cell capacitor voltages and is controlled to be kept constant at reference V^*_{ave}.

The outer controllers' task end at the points when the active power controller produces the d-axis current reference i^*_d and the reactive power controller produces the q-axis current reference i^*_q. The inner current control results in generating the voltage vector references v^*_d and v^*_q using proportional gains (k_d, k_q). Finally, these voltage references are transformed to a three-phase voltage references through the inverse Park's transformation to be used later to determine the PWM pattern via a voltage space vector scheme.

This controller will be later replaced with a VSG control to compare their effectiveness on the remote ac grid.

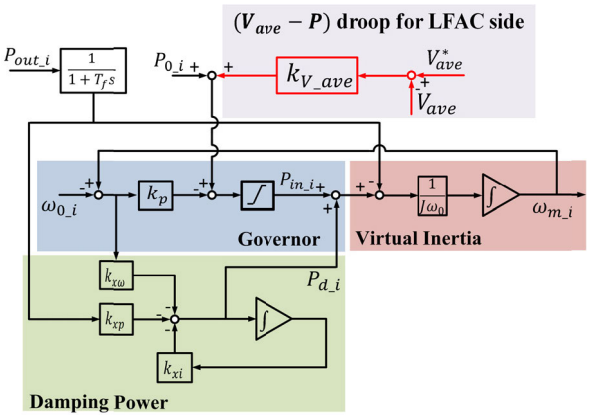

FIGURE 4. Proposed VSG control combining the governor, damping power, and the virtual inertia control scheme, and $V_{ave} - P$ droop (for LFAC side only).

As for the LFAC side control, to form a multi-terminal LFAC system, the conventional one also uses a VSG control [26]; thus, it is almost the same as the proposed one shown in Fig. 2. However, since the average dc capacitor voltage V_{ave} is controlled by the remote ac grid side, which is shown in Fig. 3, the proposed average dc capacitor voltage control discussed afterwards is not applied. Therefore, it is much easier for the conventional method to apply the VSG control in the LFAC side.

C. PROPOSED DUAL VSG CONTROL

As shown in Fig. 2, which clearly demonstrates the feature of the proposed system, two VSG control units are used in both the LFAC and the remote ac grid sides. Each VSG comprises active power-frequency (*P-f*) control part, and a reactive power control part. The M3C 1 employs a *Q-V* droop controller on its remote ac grid side, whereas an automatic voltage regulator (AVR) on its LFAC side. The *P-f* control part used for both LFAC and the remote ac grid sides of the M3C 1 is almost identical except that we chose to include the droop characteristic between the average dc capacitor voltage and active power (V_{ave}-P) to be an additional part of the LFAC side VSG controller, as shown in Figs. 2 and 4. This design is made from the following two concerns; First, when the LFAC side active power includes the (V_{ave}-P) droop, the losses of the converter within the received power from the LFAC side will be included, otherwise, the system will experience an input and output power imbalance, which results in converter cell dc capacitor voltage deviation. Second, if the active power of the remote ac grid side is set indirectly, the remote ac grid side VSG controller will choose to regulate the cell dc capacitor voltage instead of grid power. Thus, the grid power transient response will be slower because the VSG controller of the remote ac grid side will take a longer time to realize and synthesize the power change in the remote ac grid. As a result, the system will fail to support the dynamic state of the remote ac grid. In other words, the remote ac grid side VSG will not be able to quickly inject active power to mitigate the

frequency deviation and the entire LFAC link will not be able to react fast to contribute to enhancing frequency regulation.

The VSG parameters are input to the control scheme from those sides accordingly. It can be seen from Fig. 4, which represents the VSG control scheme that the input signals are included with the subscript i, referring to the LFAC or the remote ac grid side measured signals. The VSG control function comprises the swing equation, governor, and damping units. The swing equation of the VSG is

$$P_{in\_i} - P_{out\_i} + P_{d\_i} = J\omega_{0\_i}\frac{d\omega_{m\_i}}{dt} \tag{3}$$

where ω_m is the virtual rotating angular frequency, ω_0 is the nominal frequency, and P_{in}, P_{out}, P_d are the virtual shaft power produced by the governor control, the output power, and the damping power, respectively. J is the moment of inertia of rotating mass, which can be determined as

$$J = \frac{MS_{base}}{\omega_0^2} \tag{4}$$

where M is the inertia time constant, S_{base} *is* the rated MVA of the M3C.

The damping power P_d is generated by a state feedback control loop as follows [9]

$$P_{d\_i} = -k_{x\omega}(\omega_m - \omega_0) - k_{xP}\frac{1}{1+T_f s}P_{out} - k_{xi}\frac{1}{s}P_{d\_i} \tag{5}$$

where $k_{x\omega}$, k_{xp}, and k_{xi} are the feedback gains of virtual rotor frequency, output active power, integral term of P_d; and T_f is the time constant of the low-pass filter (LPF), VSG control parameters are given in Table 1. The used damping method allows the designer to avoid using the PLL for detecting the frequency, as applied in some previous methods [10], [11]. By rearranging (3), the virtual mechanical frequency is thus

$$\omega_{m\_i} = \frac{1}{J\omega_0}\int (P_{in\_i} - P_{out\_i} + P_{d\_i})dt \tag{6}$$

where, the obtained virtual angular frequency ω_m is then integrated to generate the phase angle θ_{m_i} to form a three-phase reference voltage for the LFAC and the grid sides. The design of VSG control parameters is explained in [9], [12].

The governor control part of the VSG, shown in Fig. 5, is working based on the ω-P droop characteristic. It is preferable to use the ω-P droop control especially when the system is highly inductive like traditional SG. Moreover, conventional droop control is used for the sending terminal (M3C 2) whereas a reversed droop control is used for the receiving terminal (M3C 1) as explained in [26]. The conventional and reversed governor control produce the shaft power P_{in} as follows

$$\begin{aligned} P_{in} &= P_0 - k_p(\omega_m - \omega_0)\ \text{(conventional)} \\ P_{in} &= P_0 + k_p(\omega_m - \omega_0)\ \text{(reversed)} \end{aligned} \tag{7}$$

where P_0 is the commanded value of active power, k_p is the droop coefficient, ω_0 is the nominal frequency [10], [13]. The droop term is chosen to allow 5% change of frequency as a response to a full active power change and it was set in per unit value, calculated as

$$k_{p\_pu} = \frac{k_p\omega_0}{S_{base}} \tag{8}$$

TABLE 1. Parameters of M3C 1.

Common Parameters	
Parameter	Value
Rated M3C power S_{M3C}	200 MVA
$V_{base_{LFAC}}$	275 kV
V_{base_grid}	150 kV
f_{LFAC}	10 Hz
f_{grid}	60 Hz
X_{grid}	0.1 pu
X_{LFAC}	0.016 pu
M3C Parameters	
Parameter	Value
Sampling frequency	2 kHz
Capacitor voltage	128 kV
Cell capacitor	0.69 s
Arm inductor	0.008 pu
Q-V droop and AVR PI Controllers Parameters	
Parameter	Value
K_p	0.2 pu
K_i	0.5 s
K_{q_pu}	10 pu
Stator Impedance Adjuster and Current Limiter Parameters	
Parameter	Value
LFAC side L_{ls0}	0.541pu
Grid side L_{ls0}	0.569 pu
k_z	1

VSG Parameters		
	LFAC side VSG	Grid side VSG
Parameter	Value	Value
V_{base}	275 kV	275 kV
P_{0_pu}	1 pu	1 pu
ω_0	62.8315 rad/s	376.9911 rad/s
M	8 s	8 s
k_{p_pu}	20 pu	20 pu
$k_{v\_ave\_pu}$	10 pu	-
T_f	0.0159 s	0.00265 s
k_{xp}	1	1
$k_{x\omega}$	91.4140 pu	202.1987 pu
k_{xi}	8.8522 s^{-1}	23.4591 s^{-1}

D. ADDITIONAL CONTROL BLOCKS ATTACHED TO THE DUAL VSG CONTROL

In order to give a detailed look at the other control parts in Fig. 2, this subsection discusses three control parts:

1) Output reactive power and voltage.
2) Stator impedance adjuster.
3) Current limiter control for the remote ac grid side.

Fig. 5(a) represents the Q-V droop control on the remote ac grid side, whereas Fig. 5(b) represents the AVR of the LFAC side. The Q-V droop controller is preferable when two parallel distributed generators (DGs) are connected at the point of common coupling in order to share the reactive power autonomously. The term "droop" is provided by the voltage difference block with a droop coefficient k_q that is selected to allow 10% variation when producing 1 pu reactive power.

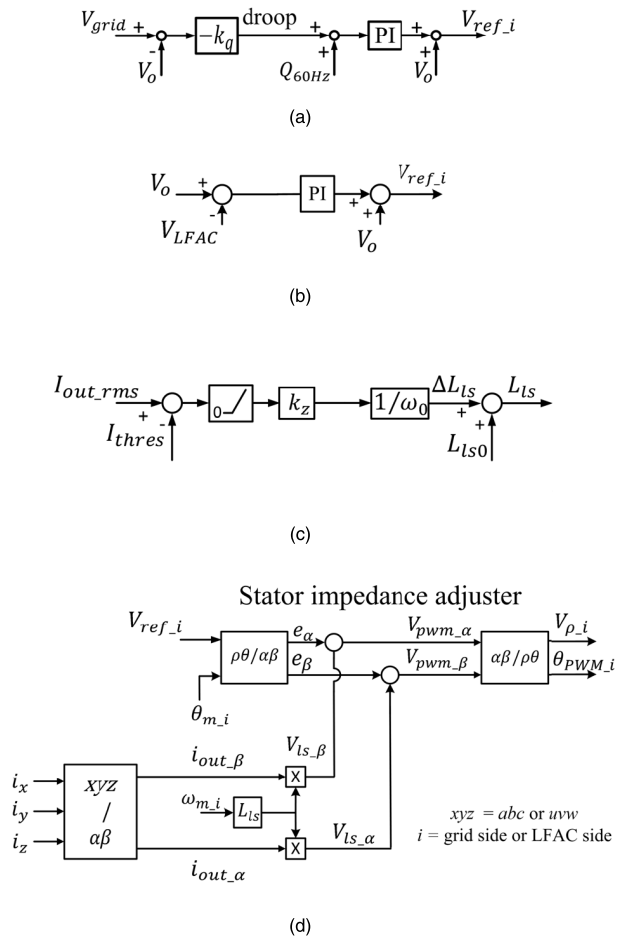

FIGURE 5. Control block of the (a) Remote ac grid side *Q-V* droop block, (b) LFAC side AVR, (c) M3C 1 current limiter control for remote ac grid side, and (d) stator impedance adjuster.

k_{q_pu} is defined as

$$k_{q\_pu} = \frac{k_q S_{base}}{V_{base}} \tag{9}$$

The AVR is used in the LFAC in order to maintain the voltage level by varying the reactive power. Whereas, the other terminal(s) in the LFAC network use an automatic reactive power regulation (AQR) in order to minimize the reactive power sharing errors, which is omitted in this paper.

The result of all controllers is V_{ref_i}, (the subscript i refers to either remote ac grid or LFAC sides parameters of each M3C), which indicates the reference voltage generated from these controllers to be used later as an input to each corresponding stator impedance adjuster block as shown in Fig. 5(d).

The stator impedance adjuster block is incorporated along with the dual VSG control in the M3C-LFAC system. Each one has a different function. For example, for the LFAC side, due to the low frequency, the X/R ratio will be 6 times smaller than that of the 60 Hz for a given rated voltage level, in which it is 1.5 in this system. Thus, the system will become less inductive [36]. Therefore, the virtual stator reactance is introduced in order to increase the total reactance of the M3C station in order to avoid the coupling between P and Q. Based on [11], a stator impedance control is applied to adjust the total output reactance of each terminal, which is calculated as

TABLE 2. Parameters of a round rotor SG.

Common Parameters	
Parameter	Value
Rated S_{SG}	200 MVA
Terminal voltage	13.8 kV
M	3.2 s
x_d, x'_d, x''_d	1.65, 0.23, 0.17
x_q, x'_q, x''_q	1.59, 0.38, 0.17
$\tau'_d, \tau''_d, \tau''_q$	0.83, 0.023, 0.023
Stator resistance R_s	2.8544e-3 pu
Governor droop coefficient R	20 pu
LFC PI controller time constant	0.5 s
Speed governor coefficient T_G	0.1 s
Turbine HP coefficient F_{HP}	0.3 s
Time constant of reheater T_{RH}	7.0 s
Time constant of main inlet volumes T_{CH}	0.2 s

$$X^* = \frac{XS_{base}}{V_{base}^2} = \frac{\omega_0 \left(L_{ls} + L_f + L_{line}\right) S_{base}}{V_{base}^2} \tag{10}$$

where, L_{ls} is the virtual stator inductance, L_f and L_{line} are the inductance of the L filter and the transmission line, respectively. From (10), L_{ls} is calculated as 0.089 pu for the LFAC side. Thus, the AVR output results are updated by the stator impedance adjuster block.

On the other hand, another function of the stator impedance is to be used to increase the converter's output impedance temporarily during an overcurrent condition (e.g. occurrence of fault) [37], as shown in Fig. 5(c). This function provides the fault ride-through (FRT) ability for a VSG control scheme, whereas, the FRT ability is realized by a current reference limiter in conventional control as shown in Fig. 3.

Finally, this controller results on generating the voltage references for the M3C space vector pulse width modulation (SVPWM) as shown in Fig. 2.

IV. SIMULATION RESULTS

To verify the proposed system, several simulation tests were carried out in PSCAD/EMTDC software environment for the system shown in Fig. 1.

M3C 2 regulates the active power received from the main grid and sends this power through a 200 km LFAC link to M3C 1 by integrating the virtual mechanical speed from the VSG to provide the phase angle. Then the LFAC side VSG control of M3C 1 regulates the active power and uses its AVR to maintain the voltage by varying the reactive power. The remote ac grid includes a conventional SG and associated loads, which represents a relatively weak system. The fixed load $P_{L1} + Q_{L1}$ is 400 MW + 100 Mvar, whereas a disturbance load $P_{L2} + Q_{L2}$ represents 5% of the fixed load and it is set to be turned on and off at specific times. These loads are being supplied by both SG and the M3C-LFAC system. The M3C 1 parameters and the SG parameters are listed in Tables 1, and 2, respectively. On the other hand,

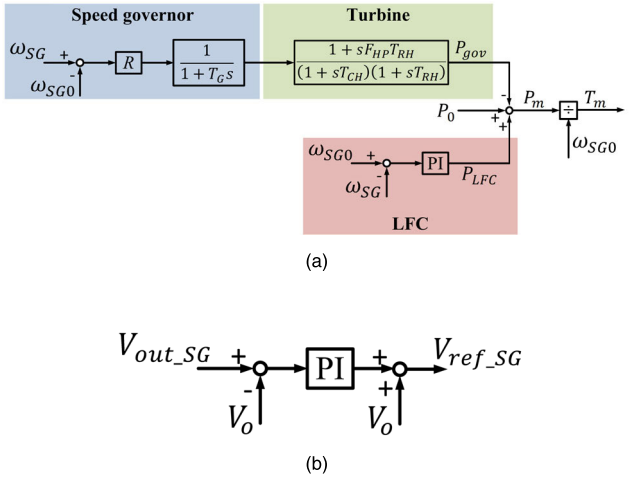

FIGURE 6. Control block of SG; (a) Speed governor, turbine model, and LFC, and (b) AVR block.

the operation of the system under conventional control is explained in [26], as discussed in Section III-B.

The SG is built by using transient and sub-transient parameters of a round rotor type obtained from [38], [39]. The conventional SG control is shown in Fig. 6. It consists of three parts, the AVR, the speed governor, and the load frequency control (LFC). The LFC is needed to regulate frequency deviations due to active load dynamic variations.

The corresponding block diagram of frequency regulation is shown in Fig. 6(a), where T_G represents the time constant of the speed governor and F_{HP}, T_{RH} and T_{CH} are the coefficients of the reheat turbine [40], these parameters values are given in Table 2. The output of this controller is the input set point of the mechanical torque (T_m) used for the SG. The AVR shown in Fig. 6(b) is employed to maintain the output voltage.

A. LOAD CHANGES

Generally, in the frequency regulation point of view, the most common disturbance in power system is load change [41]. If the power system lacks the inertia, this will lead to a large frequency deviation. This deviation, particularly if the load varies significantly, may lead to system instability.

Figs. 7 and 8 show the simulation results for a step load increase and decrease, respectively. In order to perform the load change, a switchable load $P_{L2} + Q_{L2}$ as can be seen from Fig. 1, is turned on or off, at $t = 20$ s, to perform load increase or decrease. Fig. 7(a) illustrates the SG rotor angular frequency. It can be observed that when the system is under the VSG control, the frequency nadir is reduced, and the frequency fluctuation becomes slower and smoother than that under the conventional control. After a short period of transient (which is decided by the LFC controller of the SG), the frequency of the grid can be restored to the nominal value. Thus, the VSG has improved system stability.

Figs. 7(b), (c), and (d) illustrate the active powers of the SG, and the M3C in both grid and LFAC sides, respectively. It can be noticed that the VSGs of both grid side and LFAC

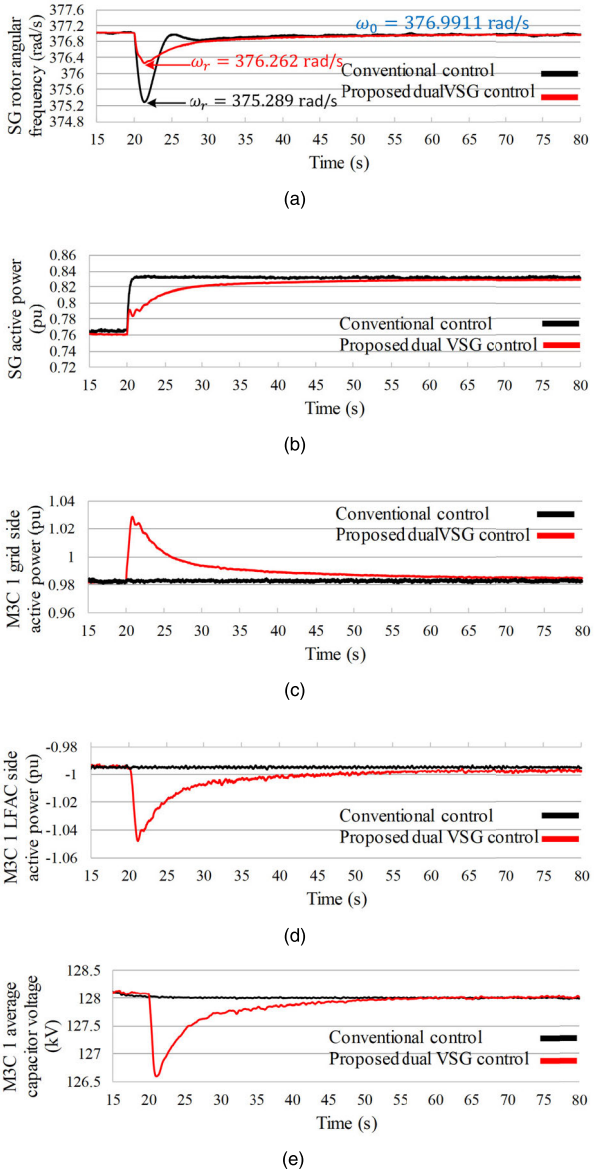

FIGURE 7. Simulation waveforms of the system with the proposed dual VSG control and with conventional control under 5% load increase: (a) SG rotor angular frequency, (b) SG active power, (c) M3C 1 grid side active power, (d) M3C 1 LFAC side active power, and (e) M3C 1 average dc capacitor voltage.

side are reacting in order to inject power into the remote ac grid to support the load increase demand. This confirms how the M3C-LFAC link can provide fast power injection response. From Fig. 7(c), it is clear that the M3C injects the required power until the SG increases its active power as shown in Fig. 7(b) to respond to the power mismatch. Similarly, the VSG on the LFAC side will request this power to be provided from M3C 2 through LFAC link. As a result, both VSGs respond accordingly to inject the required power. Once the steady-state operation is restored, the M3C-LFAC system restores its active power to the pre-transient value. It can be confirmed that all VSGs have enhanced the M3Cs with a fast response to support the frequency regulation of the remote ac grid.

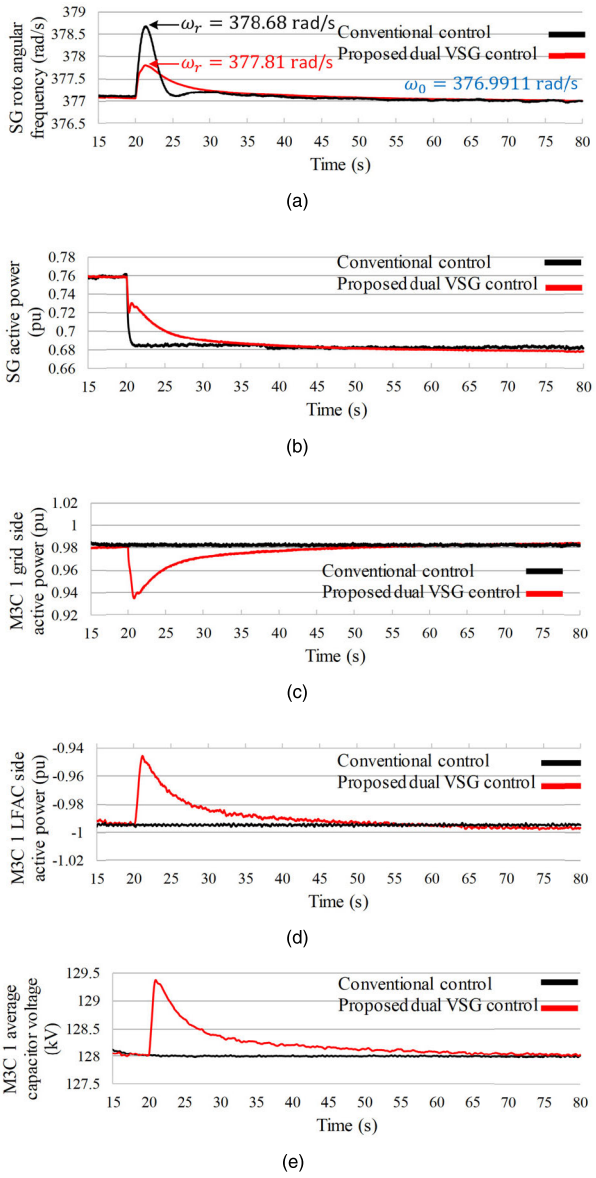

FIGURE 8. Simulation waveforms of the system with the proposed dual VSG control and with conventional control under 5% load decrease: (a) SG rotor angular frequency, (b) SG active power, (c) M3C 1 grid side active power, (d) M3C 1 LFAC side active power, and (e) M3C 1 average dc capacitor voltage.

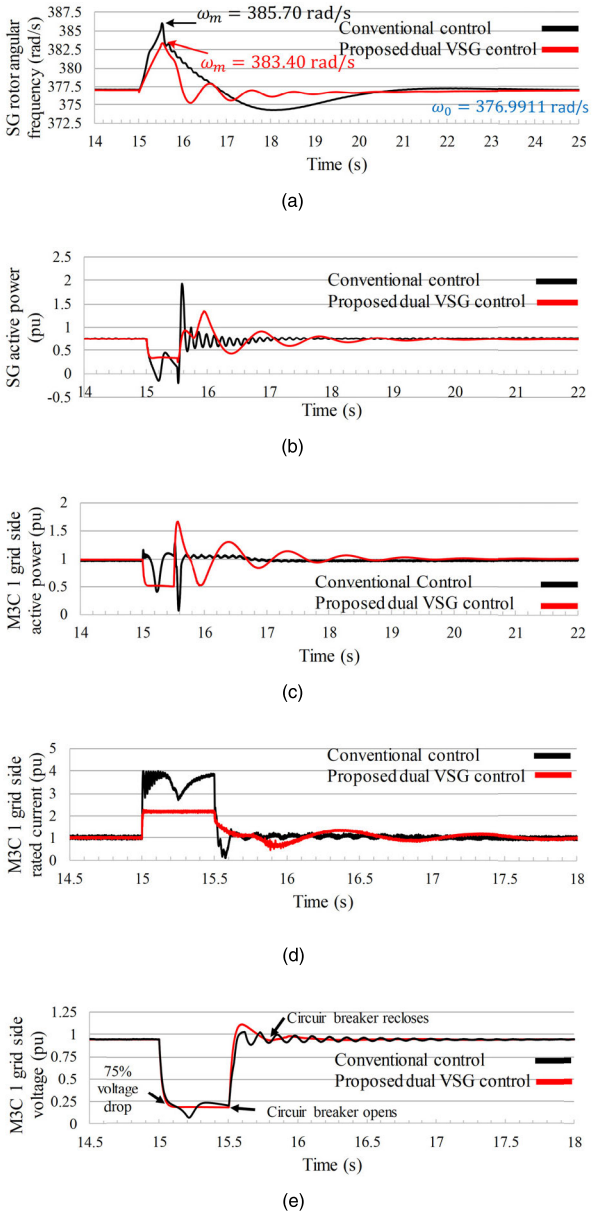

FIGURE 9. Simulation waveforms of the system with VSG control and with conventional control under 500-ms three-phase-to-ground (R_g= 5Ω) fault at the load: (a) SG rotor angular frequency, (b) SG active power, (c) M3C 1 grid side active power, (d) M3C 1 rated current, and (e) M3C 1 grid side voltage amplitude.

Fig. 8 shows the simulation results of the step load decrease scenario. This scenario is initiated by turning off the switchable load. As the case of step load increase, the VSG controller has succeeded in mitigating the frequency deviation as shown in Fig. 8(a). Figs. 8(b), (c), and (d), show the active powers of the SG, and M3C 1 grid and LFAC sides, respectively. Again, the VSG controls on both sides allow the M3C-LFAC system to respond fast to support this load reduction, compared with the conventional control that does not allow the M3C to have an inertial response.

In both load change scenarios, the VSG control has succeeded in mitigating the frequency deviation and the average dc capacitor voltage deviation is kept within 2% during transient states. Moreover, from Figs. 7(e) and 8(e), the proposed V_{ave}-P droop on the LFAC side managed to maintain the power balance between the input and the output and thus, succeeded in keeping the average dc capacitor voltage constant.

B. THREE-PHASE-to-GROUND FAULT

Fig. 9 shows a performance comparison of the M3C-LFAC system interconnecting a remote ac grid with the proposed dual VSG-based control and conventional control schemes during a fault event. A three-phase-to-ground fault (with a grounding resistance of $R_G = 5\Omega$) located at the load referring to Fig. 1, is initiated at $t = 15$ s and cleared at $t = 15.5$ s by opening the faulty line. Then, a first successful

reclosing attempt of a circuit breaker after the fault is cleared at $t = 15.7$ s (according to a typical reclosing time of an SF_6 circuit breaker [42]) occurred to bring back the line in operation.

From Fig. 9(e), the fault causes a voltage drop of about 75 % at the remote ac grid side of M3C 1. From Fig. 9(a), it is depicted that when the fault occurs, under the proposed dual VSG control with stator-impedance-based current limiting, the SG rotor angular frequency variation is mitigated compared with the conventional control. From Figs. 9(b), and 9(c), it can be seen that the VSG control enables SG and M3C 1 to maintain the power variation not to exceed 0.5 pu. On the other hand, the performance of the conventional control is not favorable, which results in large power oscillation.

Moreover, the VSG control was further enhanced to include a fault ride-through capability owing to the current limiter control scheme embedded in the stator impedance adjuster block. When the fault occurs, the control scheme is able to perform a current-limiting strategy. There is a trade-off between suppressing the fault current and the frequency deviation. It is well known that a more suppressed current results in a larger frequency deviation. Therefore, from the frequency support point of view, we choose to maintain the current at 2 pu in order to show the frequency support property of the proposed controller compared with the conventional control. On the other hand, with the conventional control, the strategy on limiting the fault current is inherited from the same strategy used with inverter-based DGs using a multi-loop control [15], by limiting the references dq components of the inner and outer conventional controller loops. However, the investigation on the M3C with conventional control taking into account the occurrence of fault as a case study still immature and requires further study. As can be seen in Fig. 9(d), the conventional control fails to limit the overcurrent within an acceptable value. The limiters of the conventional control were set to 1.06 pu. Thus, without altering the conventional control, we target the advantages of the proposed dual VSG control scheme, in this case, to provide a fault ride-through capability as well as providing the remote ac grid with dynamic frequency support.

Generally, the M3C-LFAC link based on the proposed dual VSG control strategy is more effective in increasing the system inertia, providing prompt frequency support, and thus reducing frequency deviation of low inertia grid.

V. CONCLUSION

This paper provides a frequency regulation support scheme during transients to a remote ac grid. This control scheme is proposed for M3C-LFAC system by applying a dual VSG control at the remote ac grid side M3C 1. The VSG control strategies applied to both sides of this M3C can enable both sides of the M3C to behave stably by providing virtual inertia.

From the frequency support point of view, the increased inertia can enhance the dynamic performance of a small rating remote ac grid. Moreover, on the LFAC side, the VSG control is applied to autonomously control active power and maintain the frequency stable in the steady-state. In order to address the difficulty of H-bridge cell dc capacitor average voltage regulation introduced by the dual VSG control scheme, V_{ave}-P droop control is incorporated in the LFAC side VSG control.

The effectiveness of the proposed dual VSG control strategy for the M3C-LFAC system is demonstrated by the time-domain simulation studies performed in the PSCAD/EMTDC software environment. It is shown that the proposed control scheme significantly outperforms its conventional counterpart.

REFERENCES

[1] K. Meah and S. Ula, "Comparative evaluation of HVDC and HVAC transmission systems," in *Proc. IEEE Power Eng. Soc. Gen. Meeting*, Jun. 2007, pp. 1–5.

[2] D. Jovcic, D. van Hertem, K. Linden, J.-P. Taisne, and W. Grieshaber, "Feasibility of DC transmission networks," in *Proc. 2nd IEEE PES Int. Conf. Exhib. Innov. Smart Grid Technol.*, Dec. 2011, pp. 1–8.

[3] J. Zhu, C. D. Booth, G. P. Adam, A. J. Roscoe, and C. G. Bright, "Inertia emulation control strategy for VSC-HVDC transmission systems," *IEEE Trans. Power Syst.*, vol. 28, no. 2, pp. 1277–1287, May 2013.

[4] M. Zhang, X. Yuan, and J. Hu, "Inertia and primary frequency provisions of PLL-synchronized VSC HVDC when attached to islanded AC system," *IEEE Trans. Power Syst.*, vol. 33, no. 4, pp. 4179–4188, Jul. 2018.

[5] M. Guan, W. Pan, J. Zhang, Q. Hao, J. Cheng, and X. Zheng, "Synchronous generator emulation control strategy for voltage source converter (VSC) stations," *IEEE Trans. Power Syst.*, vol. 30, no. 6, pp. 3093–3101, Nov. 2015.

[6] L. M. Castro and E. Acha, "On the provision of frequency regulation in low inertia AC grids using HVDC systems," *IEEE Trans. Smart Grid*, vol. 7, no. 6, pp. 2680–2690, Nov. 2016.

[7] J. Driesen and K. Visscher, "Virtual synchronous generators," in *Proc. IEEE Power Energy Soc. Gen. Meeting-Convers. Del. Electr. Energy 21st Century*, Pittsburgh, PA, USA, Jul. 2008, pp. 1–3.

[8] H.-P. Beck and R. Hesse, "Virtual synchronous machine," in *Proc. 9th Int. Conf. Electr. Power Qual. Utilisation*, Barcelona, Spain, Oct. 2007, pp. 1–6.

[9] J. Liu, Y. Miura, and T. Ise, "Fixed-parameter damping methods of virtual synchronous generator control using state feedback," *IEEE Access*, vol. 7, pp. 99177–99190, 2019.

[10] T. Shintai, Y. Miura, and T. Ise, "Oscillation damping of a distributed generator using a virtual synchronous generator," *IEEE Trans. Power Del.*, vol. 29, no. 2, pp. 668–676, Apr. 2014.

[11] J. Liu, Y. Miura, H. Bevrani, and T. Ise, "Enhanced virtual synchronous generator control for parallel inverters in microgrids," *IEEE Trans. Smart Grid*, vol. 8, no. 5, pp. 2268–2277, Sep. 2017.

[12] J. Liu, Y. Miura, and T. Ise, "Comparison of dynamic characteristics between virtual synchronous generator and droop control in inverter-based distributed generators," *IEEE Trans. Power Electron.*, vol. 31, no. 5, pp. 3600–3611, May 2016.

[13] K. Sakimoto, Y. Miura, and T. Ise, "Stabilization of a power system including inverter type distributed generators by the virtual synchronous generator," *IEEJ Trans. Power Energy*, vol. 132, no. 4, pp. 341–349, 2012.

[14] Y. Hirase, K. Sugimoto, K. Sakimoto, and T. Ise, "Analysis of resonance in microgrids and effects of system frequency stabilization using a virtual synchronous generator," *IEEE J. Emerg. Sel. Topics Power Electron.*, vol. 4, no. 4, pp. 1287–1298, Dec. 2016.

[15] J. Jongudomkarn, J. Liu, and T. Ise, "Virtual synchronous generator control with reliable fault ride-through ability: A solution based on finite-set model predictive control," *IEEE J. Emerg. Sel. Topics Power Electron.*, Sep. 23, 2019, early access, doi: 10.1109/JESTPE.2019.2942943.

[16] J. Liu, Y. Miura, H. Bevrani, and T. Ise, "A unified modeling method of virtual synchronous generator for Multi-Operation-Mode analyses," *IEEE J. Emerg. Sel. Topics Power Electron.*, Jan. 28, 2020, early access, doi: 10.1109/JESTPE.2020.2970025.

[17] L. Huang, H. Xin, and Z. Wang, "Damping low-frequency oscillations through VSC-HVdc stations operated as virtual synchronous machines," *IEEE Trans. Power Electron.*, vol. 34, no. 6, pp. 5803–5818, Jun. 2019.
[18] P. Mitra, L. Zhang, and L. Harnefors, "Offshore wind integration to a weak grid by VSC-HVDC links using power-synchronization control: A case study," *IEEE Trans. Power Del.*, vol. 29, no. 1, pp. 453–461, Feb. 2014.
[19] Y. Wen, C. Y. Chung, and X. Ye, "Enhancing frequency stability of asynchronous grids interconnected with HVDC links," *IEEE Trans. Power Syst.*, vol. 33, no. 2, pp. 1800–1810, Mar. 2018.
[20] G. Tang, Z. He, and H. Pang, "Discussion on applying the VSC-HVDC technology in global energy interconnection," *Smart Grid*, vol. 4, no. 2, pp. 116–123, Feb. 2016.
[21] C. M. Franck, "HVDC circuit breakers: A review identifying future research needs," *IEEE Trans. Power Del.*, vol. 26, no. 2, pp. 998–1007, Apr. 2011.
[22] X. Wang and X. Wang, "Feasibility study of fractional frequency transmission system," *IEEE Trans. Power Syst.*, vol. 11, no. 2, pp. 962–967, May 1996.
[23] T. Funaki and K. Matsuura, "Feasibility of the low frequency AC transmission," in *Proc. IEEE Power Eng. Soc. Winter Meeting. Conf.*, Singapore, vol. 4, Jan. 2000, pp. 2693–2698.
[24] W. Fischer, R. Braun, and I. Erlich, "Low frequency high voltage offshore grid for transmission of renewable power," in *Proc. 3rd IEEE PES Innov. Smart Grid Technol. Eur. (ISGT Europe)*, Oct. 2012, vol. 1, no. 6, pp. 14–17.
[25] W. Xifan, C. Chengjun, and Z. Zhichao, "Experiment on fractional frequency transmission system," *IEEE Trans. Power Syst.*, vol. 21, no. 1, pp. 372–377, Feb. 2006.
[26] M. Al-Tameemi, Y. Miura, J. Liu, H. Bevrani, and T. Ise, "A novel control scheme for multi-terminal low-frequency AC electrical energy transmission systems using modular multilevel matrix converters and virtual synchronous generator concept," *Energies*, vol. 13, no. 3, p. 747, 2020.
[27] S. Liu, X. Wang, L. Ning, B. Wang, M. Lu, and C. Shao, "Integrating offshore wind power via fractional frequency transmission system," *IEEE Trans. Power Del.*, vol. 32, no. 3, pp. 1253–1261, Jun. 2017.
[28] Q. Nguyen, G. Todeschini, and S. Santoso, "Power flow in a multi-frequency HVac and HVdc system: Formulation, solution, and validation," *IEEE Trans. Power Syst.*, vol. 34, no. 4, pp. 2487–2497, Jul. 2019.
[29] H. Chen, M. H. Johnson, and D. C. Aliprantis, "Low-frequency AC transmission for offshore wind power," *IEEE Trans. Power Del.*, vol. 28, no. 4, pp. 2236–2244, Oct. 2013.
[30] A. Pichetjamroen and T. Ise, "Power control of low frequency AC transmission systems using cycloconverters with virtual synchronous generator control," *Energies*, vol. 10, no. 1, p. 34, 2017.
[31] E. Olsen, U. Axelsson, and A. Canelhas, "Low frequency AC transmission on large scale offshore wind power plants, achieving the best from two worlds," in *Proc. 13th Wind Integr. Workshop*, Berlin, Germany, Nov. 2014, pp. 1–6.
[32] R. W. Erickson and O. A. Al-Naseem, "A new family of matrix converters," in *Proc. 27th Annu. Conf. IEEE Ind. Electron. Soc. (IECON)*, Nov./Dec. 2001, pp. 1515–1520.
[33] S. Liu, X. Wang, Y. Meng, P. Sun, H. Luo, and B. Wang, "A decoupled control strategy of modular multilevel matrix converter for fractional frequency transmission system," *IEEE Trans. Power Del.*, vol. 32, no. 4, pp. 2111–2121, Aug. 2017.
[34] Y. Miura, T. Mizutani, M. Ito, and T. Ise, "Modular multilevel matrix converter for low frequency AC transmission," in *Proc. IEEE 10th Int. Conf. Power Electron. Drive Syst. (PEDS)*, Apr. 2013, pp. 1079–1084.
[35] W. Kawamura, K.-L. Chen, M. Hagiwara, and H. Akagi, "A low-speed, high-torque motor drive using a modular multilevel cascade converter based on triple-star bridge cells (MMCC-TSBC)," *IEEE Trans. Ind. Appl.*, vol. 51, no. 5, pp. 3965–3974, Sep. 2015.
[36] T. Ngo, M. Lwin, and S. Santoso, "Steady-state analysis and performance of low frequency AC transmission lines," *IEEE Trans. Power Syst.*, vol. 31, no. 5, pp. 3873–3880, Sep. 2016.
[37] J. Liu, Y. Miura, and T. Ise, "Power quality improvement of microgrids by virtual synchronous generator control," in *Proc. Electric Power Qual. Supply Rel. (PQ)*, Aug. 2016, pp. 119–124.
[38] J. Machwiski, J. W. Bialek, and J. R. Bumby, *Power System Dynamics Stability and Control*, 2nd ed. Chichester, U.K.: Wiley, 2008.
[39] J. Fang, H. Li, Y. Tang, and F. Blaabjerg, "Distributed power system virtual inertia implemented by grid-connected power converters," *IEEE Trans. Power Electron.*, vol. 33, no. 10, pp. 8488–8499, Oct. 2018.
[40] P. Anderson and A. A. Fouad, *Power System Control and Stability*. Ames, IA, USA: Iowa State Univ. Press, 1977.
[41] H. Bevrani, *Robust Power System Frequency Control*, 2nd ed. New York, NJ, USA: Springer, 2014.
[42] M. Bamber *et al.*, *Network Protection & Automation Guide*, 3rd ed. Paris, France: Alstom Grid, 2011.

MUSTAFA AL-TAMEEMI received the B.S. degree in electrical engineering from the University of Technology, Baghdad, Iraq, in 2007, and the M.S. degree from Bharati Vidyapeeth University, Pune, India, in 2013. He is currently pursuing the Ph.D. degree in electrical and electronic engineering with Osaka University, Osaka, Japan. His research interests are power electronics, virtual synchronous generator, and low frequency ac transmission.

JIA LIU (Member, IEEE) received the B.Eng. and M.Eng. degrees from Xi'an Jiaotong University, Xi'an, China, in 2008 and 2011, respectively, the Dipl.Ing. degree from the University of Technology of Troyes, Troyes, France, in 2011, and the Ph.D. degree in engineering from Osaka University, Osaka, Japan, in 2016. He was with Delta Electronics (Jiangsu), Ltd., Nanjing, China, from 2011 to 2012. Since 2016, he has been with the Division of Electrical, Electronic and Information Engineering, Graduate School of Engineering, Osaka University, where he is currently an Assistant Professor. His research interests include distributed generators, microgrids, power quality, and smart loads.

HASSAN BEVRANI (Senior Member, IEEE) received the Ph.D. degree in electrical engineering from Osaka University, Japan, in 2004. He is currently a Full Professor and the Program Leader of the Smart/Micro Grids Research Center (SMGRC), University of Kurdistan (UOK). Over the years, he has worked as a Senior Research Fellow and a Visiting Professor with Osaka University, Kumamoto University, Japan, Queensland University of Technology, Australia, Kyushu Institute of Technology, Japan, Centrale Lille, France, and Technical University of Berlin, Germany. He is the author of six international books, 15 book chapters, and more than 300 journal/conference papers. His current research interests include smart grid operation and control, power systems stability and optimization, microgrid dynamics and control, and intelligent/robust control applications in power electric industry.

TOSHIFUMI ISE (Member, IEEE) received the B.Eng., M.Eng., and D.Eng. degrees in electrical engineering from Osaka University, Osaka, Japan, in 1980, 1982, and 1986, respectively. From 1986 to 1990, he was with the Nara National College of Technology, Nara, Japan. Since 1990, he had been with the Faculty of Engineering and the Graduate School of Engineering, Osaka University. He was a Professor, from August 2002 to March 2018. He is currently a Professor Emeritus with Osaka University and the President of the Nara-Gakuen Incorporated Educational Institution. His research interests are in the areas of power electronics and applied superconductivity for power systems. He is a Fellow of the Institute of Electrical Engineers of Japan (IEEJ).